# Strong interplay between giant and anisotropic magnetoresistance observed in face-centered-cubic-Co/Au multilayers between 5 and 280 K

C. Christides[a)]
*Department of Engineering Sciences, University of Patras, 265 04 Patras, Greece, and Institute of Materials Science, National Center for Scientific Research "Demokritos," 153 10 Athens, Greece*

(Received 1 August 2002; accepted 1 June 2003)

(111) oriented $[\mathrm{Co}(1\,\mathrm{nm})/\mathrm{Au}(2.5\,\mathrm{nm})]_{30}$ multilayers exhibit a strong thermal variation of the magnetoresistive (MR) signal between 5 and 280 K, that consists of field-direction dependent giant (GMR) and anisotropic magnetoresistance (AMR) contributions. Both, isothermal magnetization and the MR loops reveal the appearance of a canted magnetic state that accompanies the enhancement of the AMR contribution at lower temperatures. In addition, the experimental results reveal that the GMR and AMR contributions not only depend on the relative direction between the magnetic field and the current but also depend strongly on the relative direction of the field and the tilting angle of the mean easy-magnetization axis. The large differences observed in the magnetization and the MR curves of the as-made and the annealed films reveal the important role played by the field dependence of the magnetic domain correlations in the spin conductance of face-centered-cubic-Co/Au multilayers. © *2003 American Institute of Physics.*
[DOI: 10.1063/1.1593804]

## I. INTRODUCTION

The anisotropic (AMR) and giant magnetoresistance (GMR) effects in thin magnetic structures are one of the hottest topics in magnetism today because they find widespread applications as magnetic sensors or magnetic storage devices.[1] Usually, the AMR effect is referred to as the resistivity of a saturated polycrystalline ferromagnet (FM) that is determined[2] by the angle $\theta$ between the current density $J$ and the magnetization $M$: $\rho=\rho_{\perp}+(\rho_{\parallel}-\rho_{\perp})\cos^2\theta$, where $\rho_{\parallel}$ ($\rho_{\perp}$) is the resistivity in a direction with $J$ parallel (perpendicular) to $M$ and the $\cos^2\theta$ dependence results from averaging over all crystal orientations. When the external magnetic field $H$ is swept through the range $-H_s<H<H_s$ ($H_s$ is the saturation field) either a resistance minimum or maximum occurs, depending on the angle $\theta$. This reflects the evolution of a multidomain state to a single domain state. The GMR effect is referred to as resistance changes when the magnetic alignment of adjacent FM layers separated by nonmagnetic material (NM) is varied.[1] Both, the AMR and GMR effects follow the magnetization reversal features that appear in $M-H$ loops. However, the GMR effect occurs in a material only if under the influence of an applied field $H$ the spatial variation of the magnetization direction is changed on a scale smaller than a certain critical length, which depends on the measurement geometry.[3] Specifically, in the current-in-plane (CIP) and the current-perpendicular-plane geometries the critical lengths are given by the spin-dependent electron mean-free paths[1,4] $\lambda^{\sigma}$ ($\sigma=\uparrow$ or $\downarrow$) and by the spin–flip diffusion length[5] $\Lambda_{sd}$, respectively.

First, Rijks *et al.*[6] argued that in GMR systems, the scattering within the FM layers is anisotropic as a result of the AMR effect. Additional proof that the GMR is not isotropic has been obtained in spin valves[7] and polycrystalline multilayers,[8,9] indicating that anisotropic-GMR (AGMR) is due to the angular anisotropy of the conduction electron mean-free paths in the FM layers (the origin of the AMR effect). This leads to an interference between the GMR and AMR effects, indicating that[7,8] AGMR is mainly due to bulk spin-dependent scattering (SDS) in FM layers and not due to current shunting or internal reflection[8] in the NM layers. However, there is a number of studies[10–14] for epitaxial Co/NM superlattices (NM=Re, Cr, Cu) and bilayer films[15] showing that this additional AMR contribution not only depends on the relative direction between the magnetic field and the current but also depends strongly on the relative direction of the field and the *in-plane* easy axis, Co[0001], in the hexagonal-close-packed (hcp) phase of Co. This case is of particular technological interest because the epitaxial growth of coherent hcp-Co layers with in-plane $c$-axis orientation can control both, the symmetry of the in-plane magnetic anisotropy and the interlayer coupling strength [and therefore the magnetoresistance (MR)] in Co-based superlattices. Some studies in epitaxial[12] Co/Cu(111) and perpendicular magnetic Co/Au multilayers[9] have shown that: (1) the observed AMR effect is due to scattering from the hcp stacking in Co, (2) the observed correlations between AMR and hcp-Co could be owed[12] to the anisotropic effect of the two-fold uniaxial anisotropy along the Co[0001] $c$ axis, and (3) the observed differences[13,14,16] in GMR amplitudes depend on the epitaxial relationship between the hcp-Co layer and the spacer-layer crystalline directions. However, substantial differences were reported[13,14,16] for the GMR and AMR contributions in epitaxial hcp-Co/Cr superlattices that exhibit a strong four-fold in-plane anisotropy. This four-fold anisotropy creates[14] a considerable biquadratic interlayer coupling

a)Electronic mail: christides@ims.demokritos.gr

 

$J_{biq}$. Since at certain regions of spacer-layer thickness[17,18] the biquadratic coupling can be greater than the bilinear exchange coupling $J_{bil}$ then the strength of $J_{biq}$ can strongly affect[1] the spin-dependent *reflection* coefficients at the interfaces (interlayer coupling) and the spin-dependent *diffuse* scattering (GMR amplitude) at the interfaces or the bulk of the FM layers.

The present study reveals a strong interplay between AMR and GMR contributions as a function of temperature in strongly (111)-textured $[Co(1\ nm)/Au(2.5\ nm)]_{30}$ multilayers. The temperature dependence of isothermal CIP-MR loops reveals a strong thermal variation of the MR signal, that consists of field-direction-dependent GMR and AMR contributions whereas the isothermal magnetization $(M-H)$ loop shapes reveal an enhancement of the biquadratic interlayer coupling that accompanies the increase of the AMR signal below 200 K. However, face-centered-cubic (fcc)-Co/Cu multilayers with strong biquadratic coupling exhibit only the GMR effect.[19,20] This indicates that the coexistence of GMR and AMR contributions in the examined Co/Au multilayers cannot be reconciled with models[21,22] that *consider a recursion relation for the in-plane directions of magnetization vectors as a function of field*. The main feature of $[Co(1\ nm)/Au(2.5\ nm)]_{30}$ multilayers is that Co adopts an fcc lattice[23,24] with one trigonal [111] axis directed along the Au[111] axis perpendicular to the film plane, instead of an elongated hcp-Co[0001] axis.[9] This trigonal strain is much larger in $[Co(1\ nm)/Au(2.5\ nm)]_{30}$ multilayers[23,24] than in (111)-textured fcc-Co/Cu multilayers[19,20] because there is a considerable out-of-plane lattice expansion ($\sim$15%) along the Co[111] axis in Co/Au structures relative to that in Co/Cu ($\sim$2%) structures. Thus, the observed interplay between AMR and GMR contributions is indirect proof that the coexistence of the two MR signals comes from a strain-induced anisotropy along one [111] trigonal axis of Co directed normal to film plane.[25] It is shown here that such a trigonal strain is adequate to produce large differences between the transverse and the longitudinal GMR signal at ambient conditions, making these low-field GMR Co/Au multilayers suitable for use in GMR switches.

## II. EXPERIMENTAL DETAILS

$[Co(1\ nm)/Au(2.5\ nm)]_{30}$ multilayers, were grown on $Si(100)/SiN_x(70\ nm)$ $5\ mm^2$ square-shaped substrates that were thermally isolated from the water cooled supporting table during deposition. Metallic disks of 99.995% pure elements with diameter 5 cm, were used as target materials in a high vacuum Edwards (West Sussex, England) E360A sputtering system with a pair of ATOM-TECH (Middle Essex, England) 320-SE planar magnetron sputter sources. All samples were deposited in a cryogenically pumped chamber with base pressure of $2\times10^{-7}$ Torr under an Ar (99.999% pure) pressure of 3 mTorr. It is worth noting that the amorphous $SiN_x$ buffer layer provides an atomically smooth surface where the observed[23,24,26,27] (111) texture is not induced by the substrate[23] in the film. The layer thickness of Au (2.5 nm) was selected at the second antiferromagnetic (AF) maximum[24] to avoid such micromagnetic effects on magnetic hysteresis or GMR loops as those observed[28] at the first AF maximum, due to growth of pinhole defects and FM bridges in the multilayer structure. The as-made multilayers were postannealed separately inside the deposition chamber at 200 °C, and 300 °C for 1 h.

X-ray diffraction (XRD) and spin-echo nuclear magnetic resonance (NMR) spectra from the as-made[26] and the annealed[29] samples have been published elsewhere. Transmission electron microscopy (TEM) images from the as made $[Co(1\ nm)/Au(2.5\ nm)]_{30}$ sample, which exhibit the maximum[24] GMR effect, have shown[23] that Co adopts an expanded fcc lattice without misfit dislocations or extended Co–Au alloying. The NMR measurements revealed[26] a unique profile of the spin-echo intensity spectra for the as-made multilayers that could not be assigned to any of the known bulk crystalline or glassy Co structures. Thus, the complementary information from previous TEM and NMR results indicates that the herein examined Co/Au samples exhibit a highly strained Co lattice with fcc stacking. In addition, past studies for these low-field GMR Co/Au multilayers have shown that at ambient conditions, the GMR effect decreases for thicker Co layers[27] whereas for thinner Au layers (less than 1.5 nm) the GMR maximum signal, observed at 2.5 nm of Au layer thickness, transforms to a pure AMR signal.[24]

Magnetic hysteresis and GMR loops were measured with a Quantum Design MPMSR2 superconducting quantum interference device magnetometer between 5 and 280 K. CIP-MR measurements were performed with the four-point-probe method using a dc current of 10 mA. All measurements were performed by first applying the maximum positive field $H$ parallel or transverse to current flow direction and then completing the loop. Four-point-probe measurements were applied in both, square- $(5\times5\ mm^2)$ and orthogonal-shaped $(4\times12\ mm^2)$ samples. In the measurement of square-shaped samples, the connection of one current and one voltage contact can be permuted without touching or rotating the sample, no changing the direction of the applied field (see Fig. 1 in Ref. 7), ensuring that there is no contribution from the usual AMR angular dependence on field direction.[30] To ensure a better homogeneity in the current–flow direction, MR measurements were performed with orthogonal-shaped samples. The distance between the voltage-sensing leads has been kept equal to 5 mm, as in square-shaped samples. Both kinds of probes gave equivalent MR curves, indicating that inhomogeneous current spread across the film does not make a significant contribution in the MR signal of the square-shaped samples. Since MR measurements on square-shaped samples do not require sample rotation and changes in electrical contacts for parallel and transverse field geometries, all the MR loops shown in Figs. 4 and 5 come from this probe. It is worth noting that the use of lithographically defined bridges (which is preferred in epitaxial Co-based films)[10] is not necessary in our case because the Co/Au films are polycrystalline and there is no texture in the film plane.

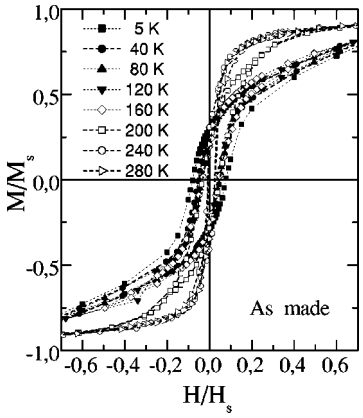


FIG. 1. Isothermal $M/M_s-H/H_s$ loops from the as-made film.

## III. EXPERIMENTAL RESULTS

### A. Magnetic measurements

Figure 1 shows normalized magnetization ($M/M_s-H/H_s$) loops between 5 and 280 K for the as-made film, with $H_s$ and $M_s$ being the saturation field and magnetization, respectively. Apparently, there is a considerable change in the loop shapes below 160 K that comes from the increase of the coercive ($H_c$) and the saturation ($H_s$) fields. Above 160 K, there is a small remanent magnetization ($M_r$) and the magnetization is approaching saturation at about $H/H_s=0.2$. Below 200 K, these loops exhibit a progressive increase of the $M_r$ and $H_c$ values with decreasing temperature (Fig. 3) whereas the magnetization is approaching saturation at about $H/H_s=0.8$. Characteristically, below 200 K, each magnetization branch exhibits a steep switching field part at small fields ($H/H_s<0.2$), where the switching near-zero field is strongly hysteretic, and a quasilinear magnetization rotation part in the interval: $0.8>H/H_s>0.2$. Figure 2 shows $M/M_s-H/H_s$ loop measurements between 5 and 280 K for the annealed sample at 200 °C. Apparently, all the loop shapes exhibit similar features without the marked changes observed in the as-made sample below 200 K. In particular, these loops exhibit lower $H_c$ values than the loops of the as-made film (Fig. 3) whereas above 200 K, each magnetization branch requires a larger field, relative to that observed in Fig. 1, to saturate the moments.

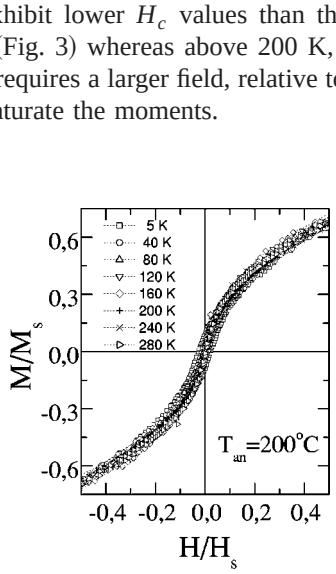


FIG. 2. Isothermal $M/M_s-H/H_s$ loops from the annealed film at 200 °C.

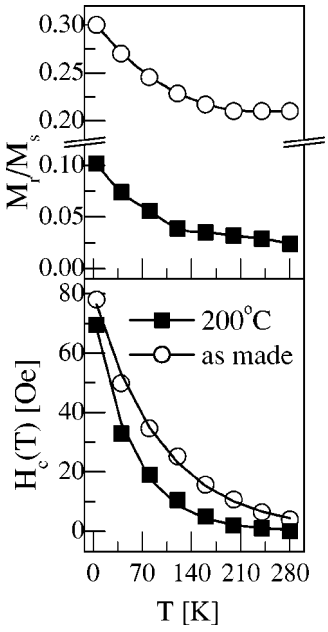


FIG. 3. The top panel shows the temperature dependence of the normalized remanence magnetization $M_r/M_s$ for the as-made (circles), and the postannealed (squares) Co/Au multilayers. The lines are guides for the eyes. The bottom panel shows the temperature dependence of coercive fields $H_c$, obtained from isothermal $M/M_s-H$ loops. The solid line is the best fit using an exponential decay function.

The observed $M-H$ loops in Figs. 1 and 2, and past hysteresis-loop measurements[24] with the field applied in-plane and perpendicular to film plane, reveal that the average magnetization is lying in the film plane for both samples, excluding the formation of stripe domain structures.[9] In addition, magneto-optical Kerr effect measurements have indicated the existence[31] of biquadratic interlayer coupling in the examined here Co/Au multilayers. Thus, it can be argued that the magnetization curves in Figs. 1 and 2 exhibit the characteristic curvature observed in[32] NiFe/Ag and[33] Fe/FeSi multilayers when the biquadratic coupling, $J_{\mathrm{biq}}<0$, satisfies the condition: $2|J_{\mathrm{biq}}|>|J_{\mathrm{bil}}|$. In this limit, the magnetization vectors among FM layers are canted[34] even at zero field (remanent state) whereas with increasing field in a $M-H$ loop, the canting angle: $\cos\Delta\theta=M(H)/M_s$, decreases up to a saturation field:[33] $H_s=-4(2J_{\mathrm{biq}}+J_{\mathrm{bil}})/M_s t_{\mathrm{FM}}$, where a parallel alignment of magnetic moments is reached ($t_{\mathrm{FM}}$ is the FM layer thickness). It is worth noting that the expression for $H_s$ can have some more additive terms in the numerator if first- and second-order ($K_1$,$K_2$) uniaxial anisotropy constants are not negligible.[14] However, reflectivity experiments with polarized neutrons[35] have shown that the magnetic phase diagrams of thin Au(111)/Co films are very complicated between 5 and 300 K because the in-plane component of the magnetization varies continuously with decreasing temperature at low fields. Specifically, it was shown[35] that different overlayers (W or Au) result in different magnetic phase diagrams because the components of magnetization perpendicular and parallel to the film plane depend on the epitaxial strain at the interfaces as a function of temperature. Furthermore, it was shown[25] that the effect of magnetic anisotropy axes in a [111]-oriented fcc-Co layer on Au(111) can

be a more complex function of anisotropy energy than that of Co[0001] when a considerable uniaxial magnetoelastic energy is induced from a strain along one (111) trigonal axis. Thus, in fcc-Co/Au multilayers, the complexity of the magnetic phase diagram[25,35] between 5 and 300 K imposes serious limitations on the applicability of the usual recursion relations[18,32,33] that estimate the biquadratic coupling from the directional cosines of in-plane magnetization vectors as a function of field.[21]

Figure 3 shows an increase of the $H_s$ and $M_r$ values below 100 K that may signify[36] a large increase of $J_{\text{biq}}$ at lower temperatures. The lower panel in Fig. 3 shows the variation of $H_c$ with temperature. An exponential decay function is used to fit the observed $H_c$: $H_c(T) = H_c(0)\exp(-\delta T)$, where $\delta$ can be associated with a blocking temperature: $\delta = 1/T_B$. Solid lines in Fig. 3 (lower panel) are least-squares fits that give: $H_c(0) = 80(5)$ Oe and $T_B = 96(6)$ K for the as-made sample, and $H_c(0) = 75(5)$ Oe and $T_B = 56(5)$ K for the postannealed sample. The obtained $T_B$'s are consisted with the progressive increase of the $M_r$ (Fig. 3 top panel) below 100 K. This behavior indicates that the magnetization reversal mechanism at low fields is associated with magnetic domains. Specifically, the observed increase of $M_r$ and $H_c$ reveals a strong variation of the micromagnetic parameters, depending on microstructural effects in the two films. Thus, the smaller $M_r$ values for the annealed film can be associated either with a more antiparallel alignment of magnetic moments in adjacent Co layers (dominance of bilinear coupling) or with a multidomain state at low fields. The GMR effect provides an additional tool for analyzing interlayer coupling, since it represents the angle enclosed by the magnetic vectors of adjacent layers rather than projections of magnetization along the field direction. Thus, the MR measurements can provide additional information for the actual micromagnetic configuration at low fields.

### B. Magnetoresistance

Figures 4 and 5 show: (1) MR loops (left-hand side axis) with the external field applied either parallel ($H \| I$, longitudinal MR) or in the plane of the film and orthogonal ($H \perp I$, transverse MR) to current ($I$) directions, and (2) the corresponding $M/M_s - H$ loops (right-hand side axis) between 5 and 280 K. The insets reveal important details at low fields. These results show a marked difference in the temperature dependence of the MR loops for the as-made and the postannealed film. The most spectacular effect is that the MR signal remains positive for small fields while for larger fields, a supplemental positive or negative MR component shows up for $H \perp I$ or $H \| I$, respectively. Such MR loops can be attributed to a combination of GMR and AMR signals because they can present either opposite signs, thus competing with each other for a specific direction of the field, or they can present similar signs, and thus reinforce each other for the orthogonal field direction.[10,11]

It is noteworthy that at all temperatures the MR curves follow the observed changes of curvature of the $M-H$ branches in both films. Figures 4 and 5 reveal two characteristic field intervals below 200 K. At low fields: $-H_c < H < H_c$, the AGMR occurs. An additional AMR component appears at the second-field interval: $|H_c| < H < |H_s|$, where the $M-H$ loops exhibit an extended curvature as well. At 200 K, the inset in Fig. 4 clearly shows: (1) the increase of $H_c$ and the change of curvature in the $M-H$ loop, (2) the increase (decrease) of hysteresis in the low-field GMR for $H \perp I$ ($H \| I$), and (3) the appearance of a wing-shaped MR component underneath the GMR signal. Below 160 K, this wing-shaped component appears either as an inverse MR signal that competes with the positive low-field GMR component for $H \| I$ or as a supplemental signal that reinforces the low-field GMR component for $H \perp I$. Below 100 K, Figs. 4 and 5 show similar AMR contributions in the total MR signal for the as-made and the annealed films.

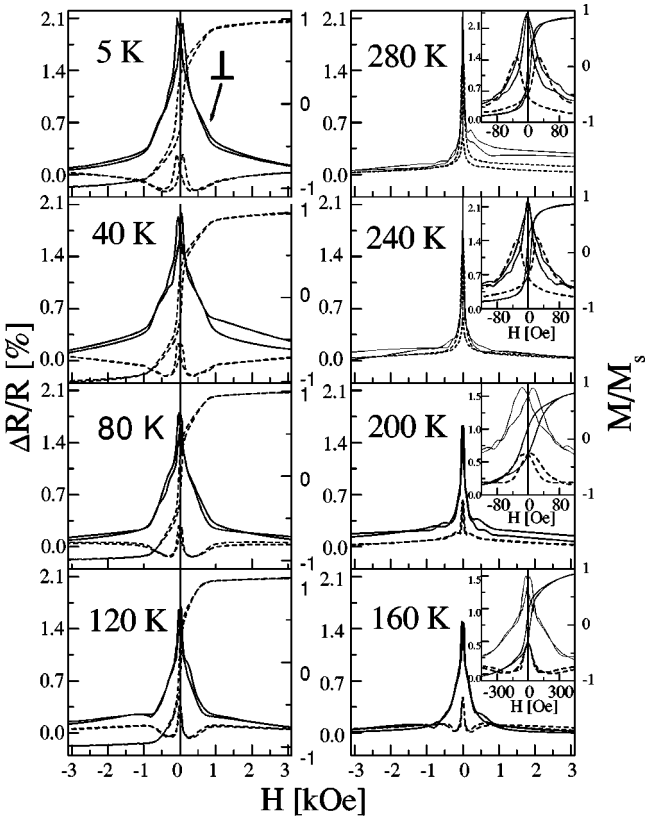


FIG. 4. Temperature dependence of isothermal magnetization $M/M_s$ (right-hand side axis) and MR (left-hand side axis) loops for the as-made film. The insets reveal important details at low fields. Solid and dashed lines show MR loops for $H \perp I$ and $H \| I$, respectively.

## IV. DISCUSSION

A study[24] of fcc-Co/Au (as-made) multilayers has shown that the AMR signal increases when the layer thickness ratio $t_{\text{Co}}/t_{\text{Au}}$ increases. It shows that the AMR effect occurs in the FM layers, as in perpendicular magnetic[9] hcp-Co/Au multilayers. However, the MR loops in fcc-Co/Au multilayers (Figs. 4 and 5) are very different from those observed[9] in hcp-Co/Au multilayers. This leads to the conclusion that the different MR curves observed in hcp-Co/Au and fcc-Co/Au multilayers are mainly due to the different stacking and the different lattice expansion of Co in the two structures.

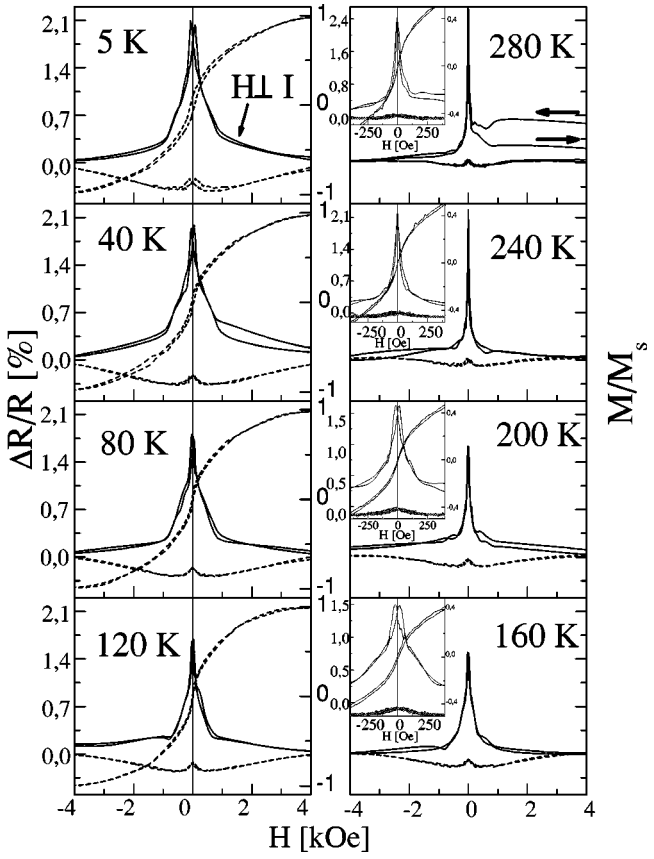


FIG. 5. Temperature dependence of isothermal magnetization $M/M_s$ (right-hand side axis) and MR (left-hand side axis) loops for the annealed film at 200 °C. The insets reveal important details at low fields. Solid and dashed lines show MR loops for $H\perp I$ and $H\|I$, respectively.

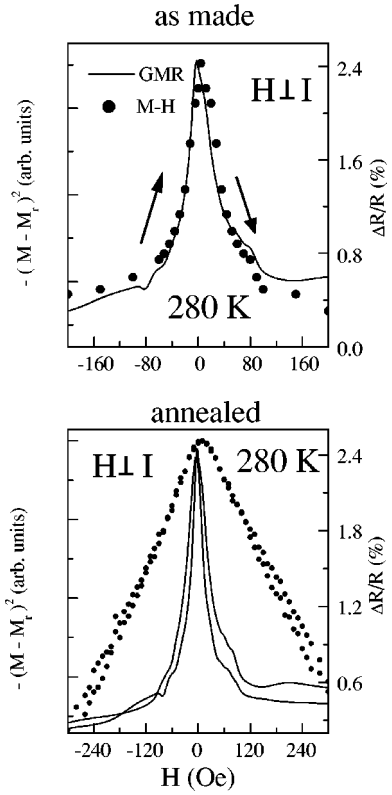


FIG. 6. Comparison between transverse MR (solid lines) and $-(M-M_r)^2$ (filled circles) vs field curves at 280 K. For clarity, the top panel shows only one branch of the MR loop for the as-made sample whereas for the $-(M-M_r)^2$ curve an $M_r=0.21M_s$ value is used from Fig. 3. The bottom panel shows a large disagreement between the MR and $-(M-M_r)^2$ curves when the $M_r=0.025M_s$ value is used from Fig. 3 for the postannealed sample.

The present study reveals some peculiar MR curves in the examined temperature range, which have never been observed in thin-film structures with mixed GMR and AMR behavior. Their peculiarity concerns the coexistence (Figs. 4 and 5) of a high-field AMR signal, that increases with decreasing temperature, with a low-field MR signal that exhibits a very anisotropic, field-direction-dependent, AGMR component above 200 K. In contrast, in all of the examined systems exhibit either[7,8] a low-field AGMR signal or the superposition of a low-field AMR component with a high-saturation-field GMR component.[9–15]

Of particular technological and fundamental importance are the large differences observed between the transverse and the longitudinal MR signals above 200 K, because this effect can be used in GMR switches. Figures 4 and 5 show that the MR loops exhibit positive $\Delta R/R_S=[R(H=0)-R(H_S)]/R(H_S)$ ratios at 280, 240, and 200 K for $H\|I$ and for $H\perp I$. $R(H_S)$ is the lowest (saturation) resistance that occurs at an $H_S\approx\pm 80$ Oe [see the insets in Figs. 4 and 5]. Such positive MR ratios for $H\|I$ and $H\perp I$ reveal a nonisotropic low-field GMR effect.[7,8] The highest GMR signal appears for the transverse configuration that exhibits the smaller hysteresis as well. This result is consistent with GMR curves observed in other AGMR systems.[7,8] Figure 5 shows that the highest GMR value ($\sim$2.7%) appears for the transverse configuration whereas the longitudinal GMR and AMR amplitudes appear negligibly small at 280 and 240 K in the annealed film. Such large differences between transverse and longitudinal MR signals have been reported[13,12] in Co/Cr superlattices as well, and their existence has been associated with a large crystalline-induced magnetic anisotropy. However, their observation in Co/Cr superlattices, and therefore their physical origin, remains a controversial matter[14] because the vertical correlation in the orientations of magnetic domains[37] (which gives rise to the resistance variation) and the mismatch of the atomic arrangement at the FM/NM interface depend on the orientation of the multilayers.

Idzerda *et al.*[37] have defined a correlation function, that represents the fraction of the film which is aligned (low resistance) minus the fraction of the film antialigned (high resistance), to quantify the vertical correlation of magnetic domains in a Co/Cr/Co trilayer. Figure 6 shows that the hysteretic behavior of the low-field AGMR signals at 280 K can be described from the field-increasing and field-decreasing branches of such a correlation function (see Fig. 3 in Ref. 37). In analogy with (111) oriented Permalloy/Au multilayers,[38] Fig. 6 shows that the $(M-M_r)^2$ profile at 280 K fits the transverse GMR profile well when the $M_r$ value is taken from Fig. 3 for the as-made sample. Thus, an $M_r=0.21M_s$ shows that this film never reaches a fully antialigned configuration and provides a direct evidence for the

presence[37] of both AF exchange coupling and FM (dipolar) coupling for different regions within the as-made multilayer. Usually, the competition of such FM and AF interactions in GMR multilayers can be described with bilinear and biquadratic contributions in the coupling energy. In this case, simulations show[21] that the shapes of the GMR profiles can vary from an inverted bell shape (parabolic) to a concave pyramid with increasing biquadratic coupling strength. Apparently, the shapes of the GMR profiles above 200 K exhibit more acute and trianglelike shapes rather than parabolic (insets in Figs. 4 and 5). Their similarity with other GMR profiles, observed in systems with considerable biquadratic coupling,[36] gives the impression that the $M-H$ and MR loops in Figs. 4 and 5 can be well accounted for by considering[21,32] a biquadratic term in the total magnetic energy.

However, there is a total disagreement between the $(M-M_r)^2$ and the GMR profiles for the annealed film (Fig. 6) when the observed value (Fig. 3) of the $M_r(=0.025M_s)$ at 280 K is used. In this case, a perfect matching of the two profiles requires a fictitious value of $M_r=0.3M_s$. Thus, the very low value of the observed $M_r$ can be explained only if we consider the presence of a multidomain configuration in the low-field region of the MR loops. In comparison, such small $M_r/M_s$ ratios have been observed and for other polycrystalline[36] or single-crystalline[34] films that exhibit a canted magnetic state due to formation of a multidomain state in the low-field region. Usually, the $M_r/M_s$ ratio is smaller for polycrystalline films because the average domain size is much smaller than that in single-crystalline films.[34] Thus, as in Co/Cr films,[14,37] the large differences observed in the magnetization and the MR data of the as-made and the annealed films reveal the important role played by the field dependence of the magnetic domain correlations in the spin conductance of fcc-Co/Au multilayers above 200 K. Since (111) oriented fcc-Co/Cu multilayers[19,20] with strong biquadratic interlayer coupling exhibit only the GMR effect between 5 and 300 K, it becomes evident that a supplementary biquadratic term in the total energy[18,21,32] of the fcc-Co/Au system is not adequate to describe the data in Figs. 4 and 5 because

(i) The large differences (Fig. 3) between the $M_r$ values of the as-made and the annealed films show that the multidomain configuration, and thus the $M_r$, should depend strongly on the characteristic columnar mode of growth observed.[23] TEM measurements have shown[23] that the as-made Co/Au multilayers exhibit a highly twinned structure where the twin planes are the (111) planes of growth. Such an extensive twinning in the (111) planes of growth can create very small bicrystalline domains due to competing anisotropies from the twinned regions. For example this situation was observed[14] in hcp-Co/Cr superlattices, where small Co domains arise from perpendicular $c$ axes oriented in registry with a four-fold symmetric substrate lattice. However, the effect of magnetic anisotropy axes in a [111] oriented fcc-Co layer can be a more complex function of anisotropy energy than that of Co[0001] if one considers the contribution of uniaxial magnetoelastic energy (ME) that is induced by the presence of a trigonal strain.[25] Considering only this cubic ME energy term[25] $K_{1,\mathrm{me}}$, the easy magnetization direction in zero field is directed along either the three–fold axes for $K_{1,\mathrm{me}}<0$, or the four-fold axes for $K_{1,\mathrm{me}}>0$. Thus, in (111)-oriented Co/Au multilayers, each crystallite can have one three-fold axis fixed perpendicular to the film surface whereas all the other equivalent axes can maintain the same angle with the film normal axis. Consequently, in multilayers with columnar grains all the other three-fold axes from the large assembly of Co crystallites should be randomly distributed and their magnetization would be lying over a conical surface. The concerted action of the conical distribution of magnetic vectors and of the competing anisotropies from the twinned regions might be the reason for the creation of a multidomain configuration at low fields. Thus, a key question underlying the magnetic behavior of these systems is the role played by the micromagnetics. In other words, to what extent is the assumption of small bicrystalline domains with strong interdomain exchange valid in the as-made and the annealed films? Neutron reflectivity measurements are planned in the near future to address such questions.

(ii) The anisotropic GMR, observed above 200 K, is an intrinsic effect due to the angular anisotropy of the spin-dependent electron mean-free paths $\lambda^{\sigma}$ ($\sigma=\uparrow$ or $\downarrow$) in the Co layers[6–8] that is proportional to the GMR ratio from bulk SDS: AGMR$\sim(\Delta\lambda^{\sigma}/\lambda^{\sigma})$GMR, plus higher-order (in GMR) terms.[8] However, the combination of the AMR and GMR contributions cannot be disentangled from the transverse and the longitudinal MR signals observed above and below 200 K because in the multilayer structure of fcc-Co/Au, there is neither a well defined uniaxial direction in the Co plane[10] nor a predefined biasing field direction orthogonal to current direction[39] to define well the conduction path.[8] Thus, an ill-defined current path[8,39] becomes a serious obstacle for the separation of the AMR component from the total MR signal because it is hard to establish the mean-free path as a function of angle between the current and the magnetization.

Thus, it becomes evident that these peculiar MR profiles cannot be simply treated by introducing a biquadratic term alone. Micromagnetic modeling of both the magnetization and the MR data in Figs. 4 and 5 requires more sophisticated experiments to better isolate anisotropy from domain coupling effects and to provide more insight into the relationship between $K_{1,\mathrm{me}}$ and the lattice expansion of Co along the [111] direction.

To investigate the effect of annealing on the microstructure, a third as-made sample was postannealed at 300 °C. Although postannealing at 300 °C further improves the interface sharpness and the (111) texture,[29] we observe that it completely suppress the GMR and AMR signals. In-plane magnetic hysteresis measurements reveal easy-plane FM

loop shapes, indicating that annealing above 200 °C creates nonconformal (uncorrelated) roughness along comparatively large lateral length scales at the interfaces which randomizes (cancels) the interactions that favor antiparallel and 90° interlayer coupling. The observed changes in the grouping of the satellite peaks around the fundamental (111)-Bragg peak of the XRD spectra[29] can be in support of such an atomic rearrangement at the interfaces as well.

In comparison, the effect of annealing on the MR properties of the examined here fcc-Co/Au multilayers is different from that observed[40] in the corresponding fcc-Co/Cu multilayers but it is closer to that observed[41] in NiFe/Cu multilayers with similar layer thicknesses. In the NiFe/Cu system,[41] the breakdown of the GMR signal starts after annealing at 220 °C and becomes zero after annealing at 300 °C due to extensive intermixing of Ni with Cu. In contrast, annealing below 220 °C causes a small increase[41] of the GMR because it improves the *magnetic homogeneity* of the multilayer. In fcc-Co/Cu multilayers postannealing up to 400 °C leads to sharper Co/Cu interfaces due to demixing of Co from Cu, and thus a continuous increase of the GMR is observed[40] due to an effective increase of the Cu interlayer thickness. Thus, the breakdown of GMR and the reduction of the AF coupling in both systems is basically related with an effective reduction of the Cu (spacer) layer thickness due to extensive diffusion of Cu at the interfaces.[41,40] Since Co and Au are not miscible materials then one expects that the observed[29] improvement of interface sharpness after annealing at 300 °C will further increase the GMR in the fcc-Co/Au system, as in[40] fcc-Co/Cu, whereas in fact a relatively early breakdown of the GMR is observed after annealing above 200 °C. The thermal stability of the GMR effect is different in fcc-Co/Au and fcc-Co/Cu multilayers because in the former: (1) the GMR effect is mainly due to bulk SDS in Co layers and thus it is not affected so much from interface roughness effects, and (2) the Co lattice is highly strained along the direction of growth thus affecting mostly the contributions from bulk SDS. In particular, it was observed[23] that the as-made sample forms an average fcc-Co–Au lattice with an interplanar lattice spacing along the growth direction that is closer to Au $d$ spacing. Thus, besides interface sharpening, postannealing above 200 °C causes a strong relaxation of the lattice parameters and the expanded $d$ spacing of the average fcc-Co–Au lattice relaxes toward the bulk $d$ spacings of the constituent elements. This destroys the magnetic homogeneity of Co and is responsible for the observed breakdown of the GMR and AMR signals after annealing above 200 °C in the fcc-Co/Au system. Further annealing, at temperatures above 400 °C leads to the formation[29] of large domains of pure Co and Au, as in fcc-Co/Cu multilayers.[41,40]

## V. CONCLUSION

In summary, this study reveals a strong interplay between the GMR and AMR effects as a function of temperature in fcc-Co/Au multilayers. Large differences are observed above 200 K between the transverse and the longitudinal GMR contributions (Figs. 4 and 5) which can find applications as GMR switches at ambient conditions. Below 200 K, there is a peculiar coexistence (Figs. 4 and 5) of a high-field AMR signal with a low-field AGMR component. A comparison of the $M-H$ loops with the corresponding MR signals reveals two characteristic field intervals below 200 K. At low-fields: $-H_c<H<H_c$, the AGMR occurs whereas an additional AMR component appears at the second field interval: $|H_c|<H<|H_s|$, where the $M-H$ loops exhibit an extended curvature. The observed combination of AMR and GMR contributions cannot be disentangled from the transverse and the longitudinal MR signals because in the multilayer structure of fcc-Co/Au, there is neither a well defined uniaxial direction in the Co plane[10] nor a biasing field direction[39] to define well the conduction path.[8] This does not allow the separation of the AMR component from the total MR signal since it is hard to establish the mean-free path as a function of angle between the current and the magnetization.[8,39] The observed interplay between AMR and GMR contributions and the temperature dependence of the $M_r$ indicate that the coexistence of the two MR signals comes from a canted magnetic state that is created from a multidomain configuration at low fields. In addition, the large differences observed in both the magnetization and MR data above 200 K (Figs. 4 and 5) for the as-made and the annealed films reveal that the micromagnetic state at low fields is determined mostly from the extensive twinning that is observed[23] in the (111) planes of growth. Thus, it becomes evident that a micromagnetic modeling of both the magnetization and the MR data in Figs. 4 and 5 requires more sophisticated experiments to better isolate anisotropy (intrinsic effect) from domain coupling effects.

[1] P. Grünberg, R. Coehoorn, and H. A. M. van den Berg, *Magnetic Multilayers and Giant Magnetoresistance*, edited by U. Hartman (Springer, Berlin, 1999), Chaps. 3, 4, and 6, respectively.
[2] T. R. McGuire and R. I. Potter, IEEE Trans. Magn. **11**, 1018 (1975).
[3] S. Zhang and P. M. Levy, Phys. Rev. B **50**, 6089 (1994).
[4] R. E. Camley and J. Barnas, Phys. Rev. Lett. **63**, 664 (1989); J. Barnas, A. Fuss, R. E. Camley, P. Grundberg, and W. Zinn, Phys. Rev. B **42**, 8110 (1990).
[5] C. Vouille, A. Barthelemy, F. E. Mpondo, A. Fert, P. A. Schroeder, S. Y. Hsu, A. Reilly, and R. Loloee, Phys. Rev. B **60**, 6710 (1999).
[6] T. G. S. M. Rijks, R. Coehoorn, M. J. M. de Jonge, and W. J. M. de Jonge, Phys. Rev. B **51**, 283 (1995); A. Granovsky, A. V. Vedayaev, and A. V. Kalitsov, Phys. Solid State **37**, 183 (1995).
[7] B. Dieny, C. Cowache, A. Nossov, P. Dauguet, J. Chaussy, and P. Gandit, J. Appl. Phys. **79**, 6370 (1996).
[8] B. H. Miller, B. P. Stojkovic, and E. D. Dahlberg, Phys. Lett. A **256**, 294 (1999).
[9] S. Honda, T. Fujimoto, and M. Nawate, J. Appl. Phys. **80**, 5175 (1996).
[10] T. Charlton and D. Lederman, Phys. Rev. B **63**, 094404 (2001).
[11] T. Charlton, J. McChesney, D. Lederman, F. Zhang, J. Z. Hilt, and M. J. Pechan, Phys. Rev. B **59**, 11897 (1999).
[12] J. C. A. Huang, Y. H. Lee, Y. M. Hu, and T. C. Chang, J. Appl. Phys. **79**, 6276 (1996).
[13] Y. Liou, J. C. A. Huang, Y. D. Yao, W. T. Liao, and C. P. Chang, J. Appl. Phys. **79**, 6282 (1996).
[14] J. J. Picconatto, M. J. Pechan, and E. E. Fullerton, J. Appl. Phys. **81**, 5058 (1997).
[15] Y. D. Yao, Y. Liou, J. C. A. Huang, S. Y. Liao, I. Klik, W. T. Yang, C. P. Chang, and C. K. Lo, J. Appl. Phys. **79**, 6533 (1996).
[16] J. C. A. Huang, Y. Liou, Y. D. Yao, C. P. Chang, S. Y. Liao, and Y. M. Hu, Phys. Rev. B **52**, R13110 (1995).
[17] R. P. Erickson, K. B. Hathaway, and J. R. Cullen, Phys. Rev. B **47**, 2626 (1993).
[18] S. O. Demokritov, J. Phys. D **31**, 925 (1998).
[19] C. Christides, J. Appl. Phys. **88**, 3552 (2000).

[20] C. Christides, S. Stavroyiannis, N. Boukos, A. Travlos, and D. Niarchos, J. Appl. Phys. **83**, 3724 (1998).
[21] C. C. Kuo, M.-T. Lin, and H. L. Huang, J. Appl. Phys. **85**, 4430 (1999).
[22] E. L. Albuquerque and M. G. Cottam, Phys. Rep. **376**, 225 (2003).
[23] T. Kehagias, P. Komninou, C. Christides, G. Nouet, S. Stavroyiannis, and T. Karakostas, J. Cryst. Growth **208**, 401 (2000).
[24] S. Stavroyiannis, C. Christides, D. Niarchos, T. Kehagias, P. Komninou, and T. Karakostas, J. Appl. Phys. **84**, 6221 (1998).
[25] M. Ayadi, R. Belhi, N. Mliki, K. Abdelmoula, J. Ferre, and J. P. Jamet, J. Magn. Magn. Mater. **247**, 215 (2002).
[26] C. Christides, S. Stavroyiannis, D. Niarchos, M. Wojcik, S. Nadolski, and E. Jedryka, Phys. Rev. B **59**, 8812 (1999).
[27] C. Christides, S. Stavroyiannis, D. Niarchos, M. Gioti, and S. Logothetidis, Phys. Rev. B **60**, 12239 (1999).
[28] K. Pettit, S. Gider, S. S. P. Parkin, and M. B. Salamon, Phys. Rev. B **56**, 7819 (1997).
[29] M. Wojcik, C. Christides, E. Jedryka, S. Nadolski, and I. Panagiotopoulos, Phys. Rev. B **63**, 012102 (2001).
[30] H. W. Zhao, M. Lu, J. Du, and H. R. Zhai, J. Appl. Phys. **82**, 485 (1997).
[31] C. Christides, R. Lopusnik, J. Mistrik, S. Stavroyiannis, and S. Visnovsky, J. Magn. Magn. Mater. **198**, 36 (1999).
[32] B. Rodmacq, K. Dumensil, P. Mangin, and M. Hennion, Phys. Rev. B **48**, 3556 (1993).
[33] E. E. Fullerton and S. D. Bader, Phys. Rev. B **53**, 5112 (1996).
[34] R. W. E. van de Kruijs, M. T. Rekveldt, H. Fredrikze, J. T. Kohlhepp, J. K. Ha, and W. J. M. de Jonge, Phys. Rev. B **65**, 064440 (2002).
[35] R. Sellmann, H. Fritzshe, H. Maletta, V. Leiner, and R. Siebrecht, Phys. Rev. B **64**, 054418 (2001).
[36] S. Colis, A. Dinia, C. Meny, P. Panissod, B. C. Ulhaq, and G. Schmerber, Phys. Rev. B **62**, 11709 (2000).
[37] Y. U. Idzerba, V. Chakarian, and J. W. Freeland, Phys. Rev. Lett. **82**, 1562 (1999).
[38] S. S. P. Parkin, R. F. C. Farrow, R. F. Marks, A. Cebollada, G. R. Harp, and R. J. Savoy, Phys. Rev. Lett. **72**, 3718 (1994).
[39] B. H. Miller, E. Y. Chen, and E. D. Dahlberg, J. Appl. Phys. **73**, 6384 (1993).
[40] L. van Loyen, D. Elefant, D. Tietjen, C. M. Schneider, M. Hecker, and J. Thomas, J. Appl. Phys. **87**, 4852 (2000).
[41] M. Hecker, D. Tietjen, H. Wendrock, C. M. Schneider, N. Cramer, L. Malkinski, R. E. Camley, and Z. Celinski, J. Magn. Magn. Mater. **247**, 62 (2002).